Enhanced photocatalytic degradation of Gd-doped Bi_2O_3 for selective dyes under UV light irradiation

E. Dhanasekaran[a], N. Sivakumar[b*], N. Sriharan[c]
[a]*Department of Chemistry, Erode Sengunthar Engineering College, Perundurai, India. Tel. +91 9629028878*
[b]*Department of Chemistry, Government Arts and Science College, Sathyamangalam, India. Tel. +91 9865302003*
[c]*Department of Physics, Erode Sengunthar Engineering College, Perundurai, India. Tel. +91 7904858681*

Nanorod like structured bare Bi_2O_3 and Gd-doped Bi_2O_3 (Gd-Bi_2O_3) are synthesized by simple hydrothermal method. The crystal structure, compositions and surface morphology of the synthesized nanoparticles are characterized by X-ray powder diffraction (XRD), Scanning electron microscopy (SEM), Energy Dispersive X-ray spectroscopy (EDS) and UV-visible absorbance spectroscopy (UV). The photocatalytic efficiency of as synthesized samples is evaluated by degradation of aqueous solution of dyes from different classes under the pH = 4, 6, 8 in presence of UV light. Comparatively, Gd-Bi_2O_3 exhibits significant degradation of dye stuffs than bare Bi_2O_3. In our present study, the factors which are emphasis the photocatalytic activity of Gd-Bi_2O_3 and possible mechanism for photocatalytic degradation also narrated briefly.

(Received December 7, 2021; Accepted June 20, 2022)

Keywords: Bismuth oxide, Gadolinium, Hydrothermal, Photocatalytic activity

1. Introduction

Over the last five decades, widespread investigations done on semiconductor photocatalysts like TiO_2, ZnO, ZnS, Cu_2O, CuS, Fe_2O_3, WO_3, SnO_2, Ag_3PO_4, $SrTiO_3$, CdS, CdSe, PdS, C_3N_4 etc., In recent days, bismuth materials drawn more attention due to wide usage in energy conversion as well as environmental applications such as waste water purification [1], photocatalysis [2], photovoltaic studies [3], antibacterial effect [4], biomedical [5,6], solid-state fuel cells, optoelectronics, optical coatings, ceramics, gas sensing [7,8] etc. Hence, researchers have been devoted to develop and emphasize bismuth based materials. Bismuth photocatalysts possess unique properties like specific surface morphology, low band gap and high photo conductivity [9]. Mainly, photocatalysts such as Bi_2O_3, Bi_2MoO_6, $Bi_{12}TiO_2$, Bi_2WO_6, $BiVO_4$, $BiPO_4$, $BiFeO_3$, BiOX (X = Br, Cl, F and I) are being investigated. In addition, photo catalytic efficiency was further enriched by doping numerous metal ions (e.g. Zn, Gd, V, Fe, Ni, Cr, Co, Ru and Pt etc.,), or non-metal ions or rare earth metal ions or as composites. In general, photo catalysts are synthesized by simple chemical methods. They are more efficient and favorable over physical methods to prepare catalysts with controlled size, shape and composition. Bismuth oxide can be prepared by using numerous chemical methodologies like solvothermal [10], laser ablation [11], hydrothermal [12], sol–gel [13], thermal decomposition [14, 15], chemical vapour deposition [16], electrode position [17] and flame spray pyrolysis [18].

The previous literature reveals that, doping of rare earth metal ions such as Eu^{3+}, La^{3+}, Nd^{3+}, Ce^{4+} and Gd^{3+} with bismuth oxide is an effective one. This approach is more attractive and enhances the photocatalytic activity under visible light and UV light. Due to the above predictable properties, the rare earth metal doped photocatalysts are used in various fields like medical science, catalysts, sensors, optoelectronic devices, magnetic resonance imaging (MRI), drug delivery, photocatalytic water-splitting and oxidation of organic dyes [19, 20]. Among them,

* Corresponding author: sukisivakumar@gmail.com
https://doi.org/10.15251/JOBM.2022.143.77

Gadolinium metal having remarkable qualities such as excellent surface modifying property with enhanced adsorbing surface morphology. It also offers low thermal stability, high chemical stability, low toxic, higher optical properties and high magnetic susceptibility. Importantly, the band gap value of Gd-doped photocatalyst is in the range of 2.90-3.30 eV. The wide band gap can make an effective barrier for recombination of photoexcited electrons after photo electron transformation to conduction band and it promotes excellent photodegradation.

In the present work, bare Bi_2O_3 and Gd-Bi_2O_3 were prepared by using simple hydrothermal method. This method offers more advantages than the other available synthesis methods, like simple handling procedure, cost effective and carried out at optimum temperature. The prepared samples are characterized by XRD, SEM with EDS and UV-Vis spectrophotometer. Furthermore, we investigated the photocatalytic degradation of selective dyes under UV light.

2. Experimental

2.1. Materials

The precursors $Bi(NO_3)_3.5H_2O$ and $Gd(NO_3)_3$ used for the synthesis are analytical grade and purchased from alfa-aesar. The selected dyes Acid Violet-19, Rhodamine-B, Direct Yellow-8 and Reactive Orange-16 are purchased from Aalfa Dyes and Chemicals (Pvt Ltd). All these chemicals were used without further purification. Double distilled (DD) water used for the preparation of stock solution, reaction mixture and the evaluation of photocatalytic degradation experiments.

2.2. Preparation of bare Bi_2O_3 and Gd-Bi_2O_3 Photocatalysts

The synthesis of bare Bi_2O_3 involves, 0.6 g of Bi $(NO_3)_3.5H_2O$ dissolved in 60 ml double distilled water with addition of 2 ml of dilute HNO_3. Then, the solution was kept under constant stirring on magnetic stirrer to get a clear solution. After that, 1.2 g of sodium hydroxide dissolved in 40 ml double distilled water was added drop wise in to the above solution with constant stirring which results the formation of yellow precipitate of bismuth oxide. The resultant solution left undisturbed without stirring, the precipitate settled at bottom and the supernatant was decanted. The precipitate was washed with double deionized water and ethanol several times, finally the obtained product was dried in vacuum oven at 60 °C for 5h. Likewise, the same procedure was used to synthesis Gd-Bi_2O_3 nanoparticles with stoichiometric proportions of $Gd(NO_3)_3$ respectively. Finally, all the prepared bare Bi_2O_3, Gd-doped Bi_2O_3 samples were annealed at 450 °C for 1h in a muffle furnace at the rate of heating 2 °C/min. Then, samples were allowed to attain room temperature by natural cooling.

2.3. Characterization techniques

The crystal structure of samples was examined by using a mini desktop X-ray diffractometer (X'PERT PRO MPD) with CuKα radiation of wavelength 1.5406 Å and a scan rate of 0.05° 2θ/s. The surface morphology and elemental composition was analyzed by using scanning electron microscope (SIGMA HV–Carl Zeiss with Bruker Quantax 200–Z10 EDS Detector) with EDS. The absorption spectra of nanoparticles are recorded using a UV–vis spectrophotometer (JASCO DB-20S). The photocatalytic activity of fabricated samples is evaluated under UV light irradiation (Philips) of 15 W with λ =365 nm.

2.4. Photocatalytic measurements

The photocatalytic degradation activity of prepared photocatalysts (bare Bi_2O_3 and Gd-Bi_2O_3) is evaluated by taking aqueous solution of selected dyes (10 ppm) with 1 g/L dosage of each photocatalysts under UV light illumination. Initially, before irradiation, the prepared suspension of all the dyes is kept in dark room for 30 m to attain the adsorption–desorption equilibrium. Then, the reaction mixture is kept under photo reactor, at a definite interval of time. About 3ml of suspension taken, centrifuged (3000 rpm, 5 min.) and filtered with 0.45 mm membrane. The absorption spectra were taken for the supernatant of the solution by UV–Vis

spectrophotometer (λmax= 580 nm). From the absorption spectra, extent of degradation is calculated.

3. Result and discussion

3.1. XRD Analysis

The crystallinity and the purity of as-prepared photocatalysts were investigated by using XRD analysis. *Figure 1(a)* shows the XRD pattern of bare Bi_2O_3 and Gd-doped Bi_2O_3 photocatalysts. It is clearly observed that all samples exhibit strong and sharp intense peak, which reveals that the high purity and crystallinity of the synthesized nanocrystals. The peaks observed at 2θ equal to 19.65°, 25.89°, 27.05°, 27.45°, 28.02°, 33.3°, 35°, 36.4°, 46.39°, 52.51° and 54.3° corresponds to (020), (002), (111), (120), (012), (200), (-212), (121), (041), (-321) and (-241) phase of monoclinic α-Bi_2O_3, which perfectly correlate with the already literally existing standard JCPDS (card no: 71-2274) of Bi_2O_3 [8]. *Figure 1(b)* shows the magnified primary peak of bare Bi_2O_3 and Gd-Bi_2O_3 samples. The major peaks observed at 2θ equal to 25.89°, 27.05°, 27.45° and 28.02° corresponds to (002), (111), (120) and (012) phase. All the major peaks are shifted towards the higher angle for the doping of Gd^{3+} ion. It may reduce size of particles. From this result, it can be concluded that the Gd^{3+} ions were incorporated into the Bi_2O_3 lattice. The average crystalline size of the bare Bi_2O_3 and Gd-Bi_2O_3 was determined by using Scherer's formula $D=K\lambda/\beta\cos\theta$ and found to be 40 and 29 nm respectively [21].

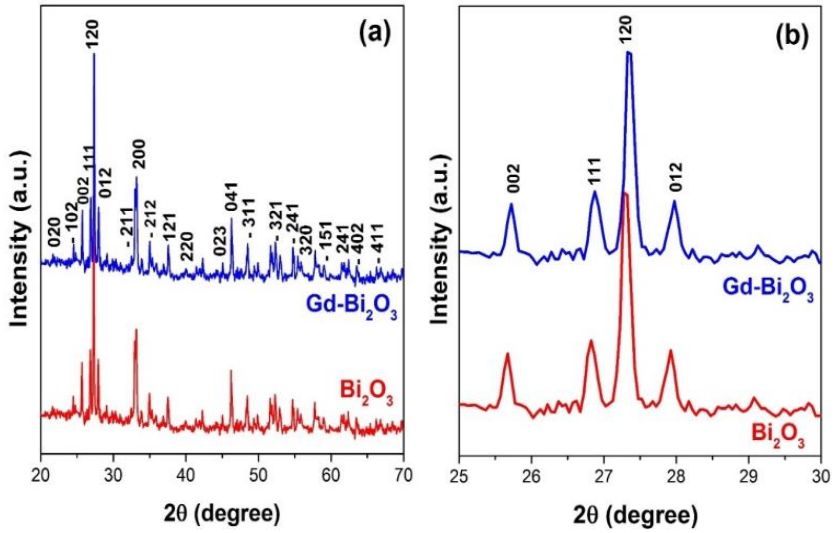

Fig. 1. XRD pattern of (a) bare Bi_2O_3 and Gd- Bi_2O_3 samples, (b) magnification of XRD primary peak shift.

3.2. SEM Analysis

Surface Morphology of the synthesized nano particles were investigated by using versatile tool Scanning Electron Microscope (SEM). The SEM images reveals about the quantum confinement effect of the synthesized materials. *Figure 2 (a-d)* shows the SEM images of the synthesized bare Bi_2O_3 and Gd- Bi_2O_3 samples. *Figure 2(a, b)* depicts the bare Bi_2O_3 has rectangular nanoparticles with different size. The average length of rectangular nanoparticles is in the range of ~110–150 nm and corresponding average diameter is ~120 nm. SEM images of Gd-doped Bi_2O_3 clearly provides the variation in morphology of the samples, shown in Figure 2 (c, d). The images clearly show that the Gd-doped nanoparticles are rod-like structure and each rod is composed of thin layers. The surface of the rod-like structure are highly porous in nature. The average length of the nano rods are in the range of ~150–210 nm with an average diameter of ~90 nm [22]. This variation of surface morphology is due to incorporation of Gd^{3+} in Bi^{3+} ions lattice.

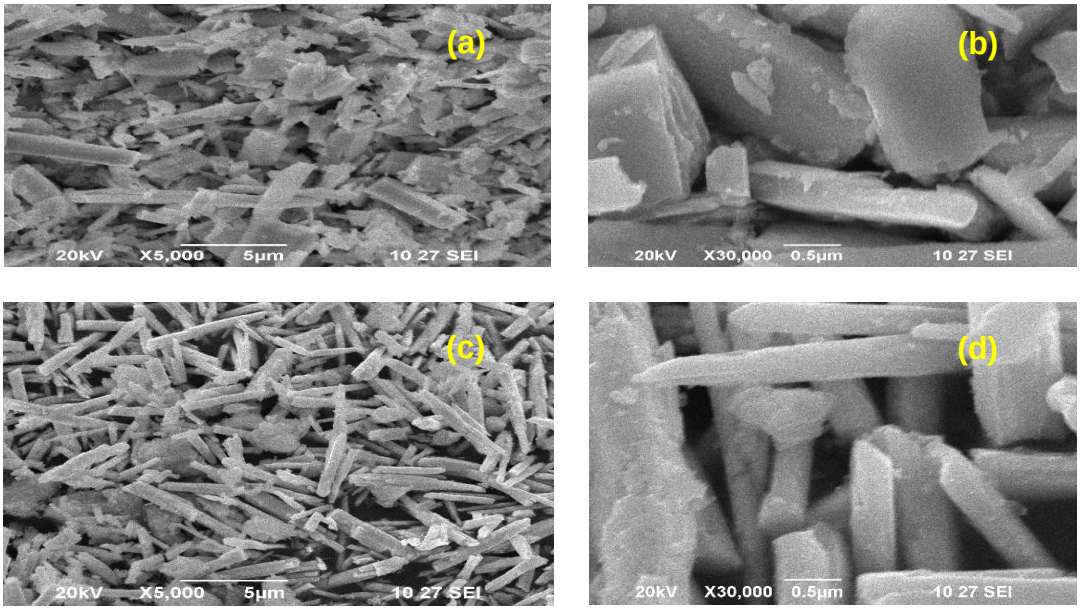

Fig. 2. SEM images of (a, b) bare Bi_2O_3, (c, d) Gd- Bi_2O_3 samples under different magnification.

3.3. EDS Analysis

The EDS analysis of bare Bi_2O_3 and Gd-doped Bi_2O_3 samples gives the stoichiometric composition of elements present in the samples. *Figure 3* gives the information about the percentage of Bi- 68.87 %, O- 31.13% in pure Bi_2O_3, Bi-21.93%, O-71.97% and Gd- 6.11 % in Gd doped Bi_2O_3. The EDS results infer no other impurities are present in the prepared samples.

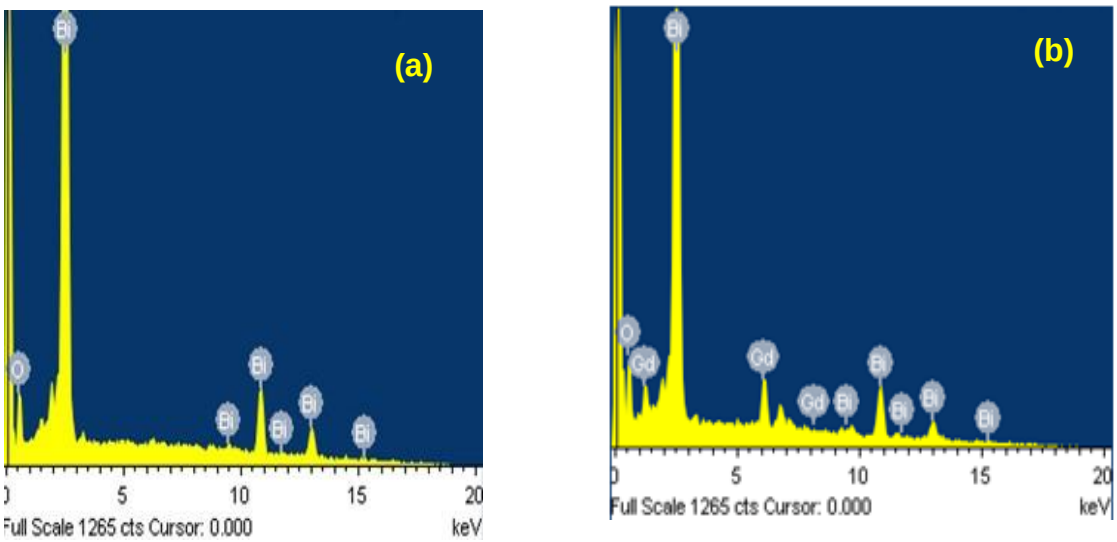

Fig. 3. EDS images of (a) bare Bi_2O_3 and (b) Gd-Bi_2O_3 samples.

3.4. UV-VIS Spectral Analysis

The optical properties of the synthesized nanoparticles were analyzed by UV-Vis absorption spectroscopy. The absorption spectra of pure Bi_2O_3 and Gd-Bi_2O_3 samples were shown in *Figure 4(a)*. It reveals that the photo-absorption edge of all analysts lays in the region in between from 420 to 470 nm. *Figure 4(b)* depicts the band gaps of the resultant samples, it can be determined by extrapolating the straight-line portion of $(\alpha h\nu)^{1/2}$ against hν plot to $\alpha = 0$ and calculated from the formula $\alpha h\nu = A(h\nu - Eg)^{1/2}$.

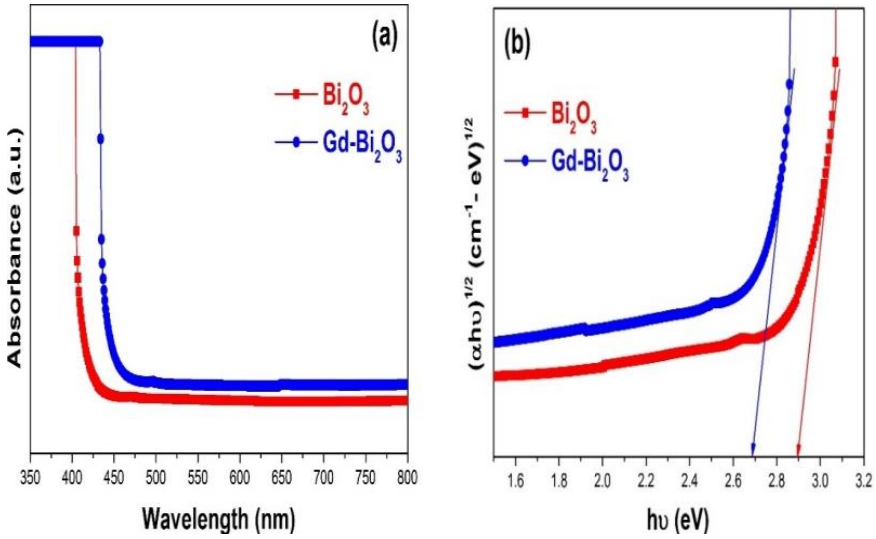

Fig. 4. UV-vis absorbance spectra of (a) bare Bi_2O_3 and Gd-Bi_2O_3 samples (b) Tauc's plot.

The resultant threshold wavelength for pure Bi_2O_3 and Gd doped Bi_2O_3 nanoparticles are 430 and 460 nm corresponding to the direct band gap values of 2.88 and.2.68 eV respectively, which strongly resides in the direct optical band gap of the monoclinic α-Bi_2O_3 of around 2.7-2.9 eV [22].

3.5. Photocatalytic Activity

Photocatalysis is the most promising techniques instead of the numerous conventional techniques available for the degradation of environmental pollutants. Especially, Bi_2O_3 is a p-type heterogeneous semiconductor, it plays important role as a photocatalysts because of its unique structures, high oxygen-ion conductivity and thermal stability. It possesses narrow band gap energy and enhances the electron-hole pair separation. It also reduces the recombination rate of the material. The photocatalytic degradative performance of as-prepared photocatalysts was evaluated under UV light illumination for the selected dyes Acid Violet-19 (545 nm), Rhodamine-B (553 nm), Direct Yellow-8 (392 nm) and Reactive Orange-16- (495 nm) and denoted as AV, RB, DY and RO. From the absorbance curve, the degradation efficiency of prepared catalysts towards the selected dyes was calculated by using the following formula.

$$\text{Degradation percentage} = ((A_0\ A_t)/A_0) \times 100\ (\%)$$

Figure 5 shows the dye degradation spectrum of bare Bi_2O_3 for the selected dyes (AV, RB, DY and RO) at pH= 4,6,8. The absorbance maximum was varying according to its extent of degradation by the catalyst. In some cases, the variation will be sudden or drastic during the light irradiation of 30 min. Generally, the degradation efficiency of the photo catalysts depends on the pH of the reaction mixture. Because, the mechanism of dye degradation depends on the availability of the initiators like h^+, OH^- and readiness of formation of other species like $^{\bullet}OH$, $HO_2^{\bullet}$ and $^{\bullet}O_2^-$. *Figure 6* shows the variation of absorption spectrum of Gd-Bi_2O_3 for the degradation of AV, RB, DY and RO dyes. It is found that the Gd-Bi_2O_3 photocatalyst shows maximum efficiency than the other catalysts. Hence, the intensity of absorbance peak was decreased linearly in short time.

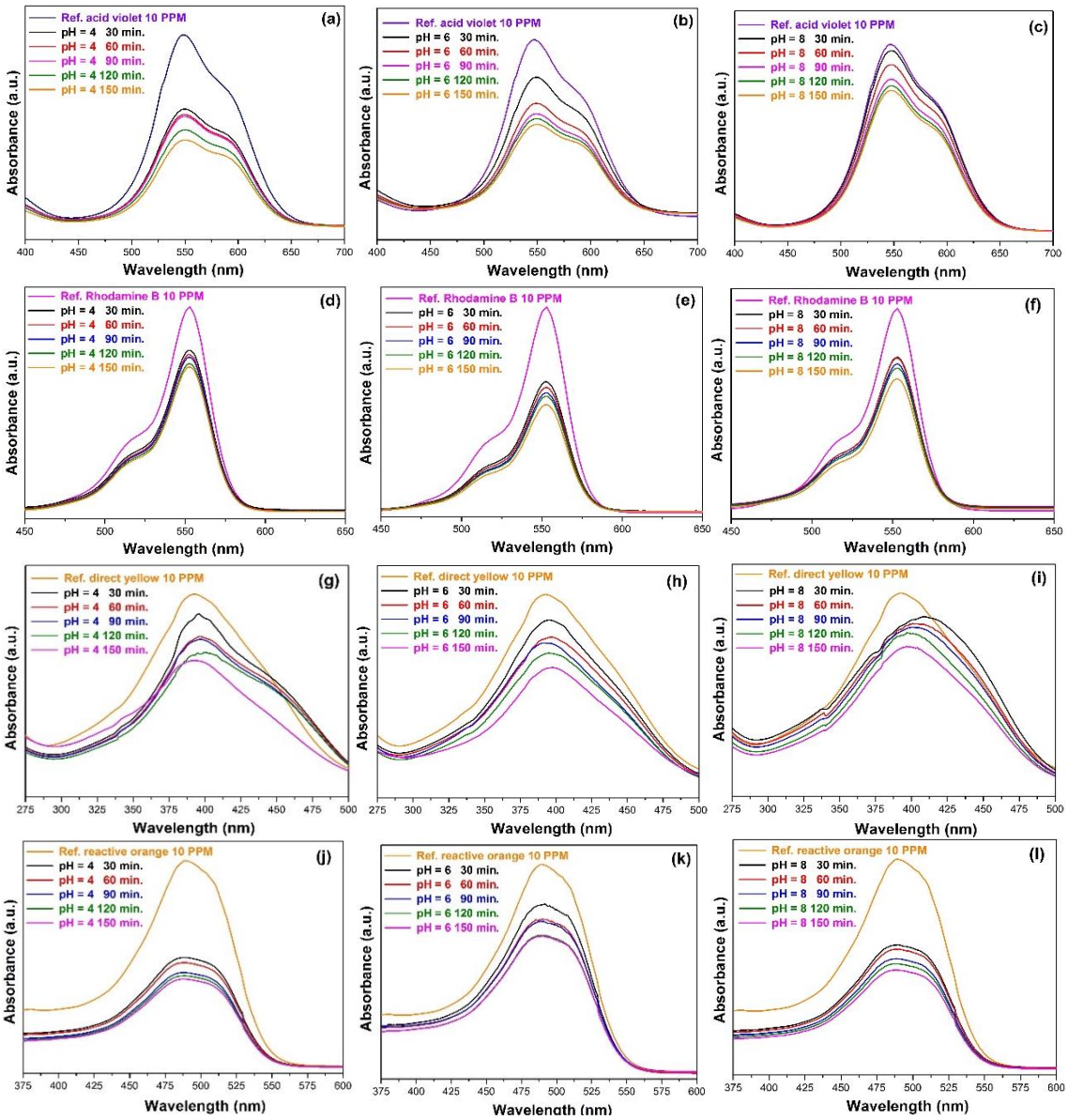

Fig. 5. UV-Visible absorption spectra of (a-c) AV, (d-f) RB, (g-i) DY and (j-l) RO dye degradation (pH- 4,6,8) by bare Bi_2O_3, respectively.

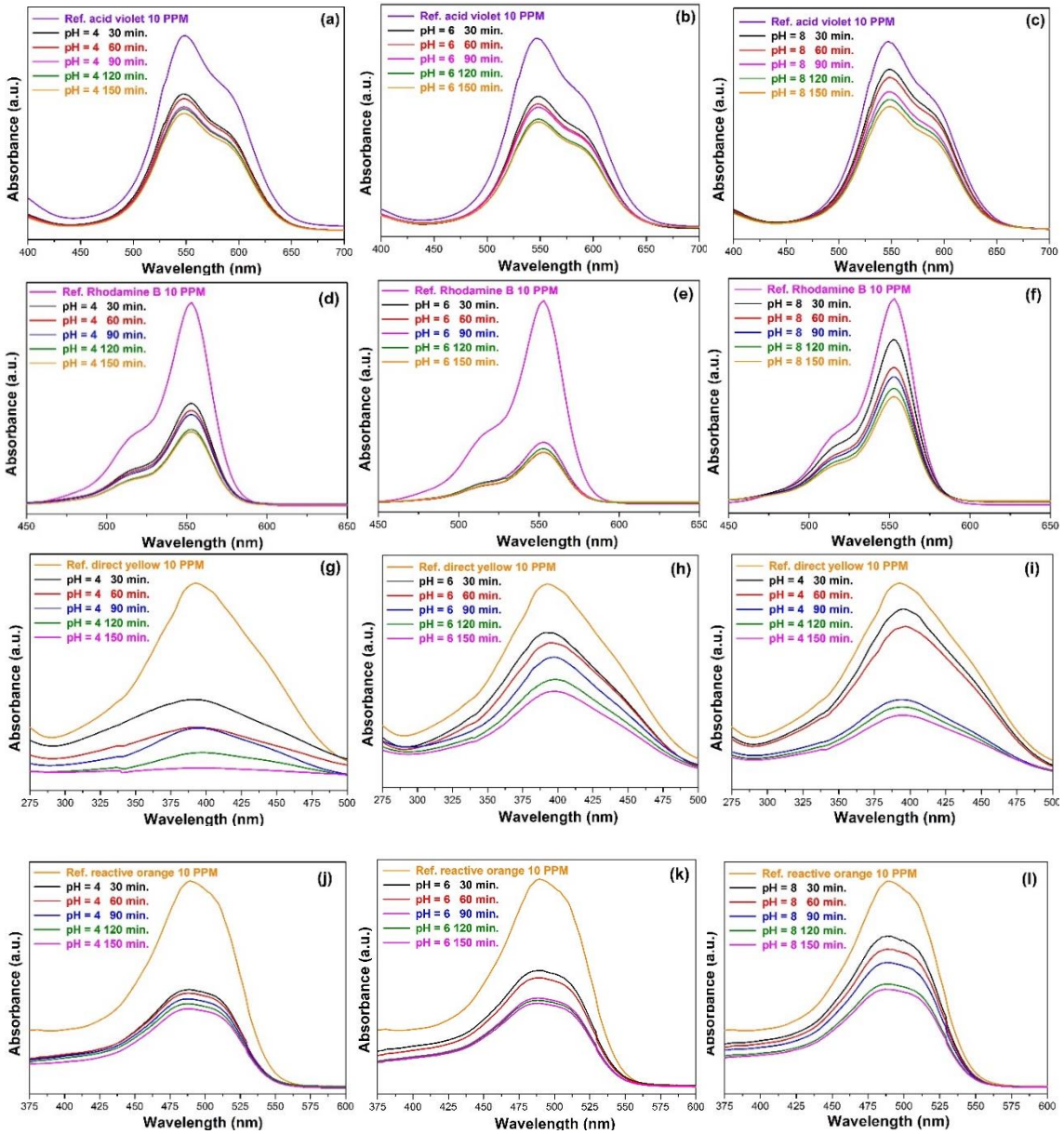

Fig. 6. UV-Visible absorption spectra of (a-c) AV, (d-f) RB, (g-i) DY and (j-l) RO dye degradation (pH-4,6,8) by Gd-Bi_2O_3, respectively.

Figure 7 shows the variation of photocatalytic efficiency of bare Bi_2O_3 for the degradation of AV, RB, DY and RO dyes. From the Table 1, it was found that AV and RO undergo average degradation than the other dyes. Under different pH conditions the availability of the initiators like h^+, OH^- and formation of other species like $^{\bullet}OH$, $HO_2^{\bullet}$ and $^{\bullet}O_2^-$ will vary. The reason for the observed low degradation efficiency of bare Bi_2O_3 is due to the easy recombination of photo induced electron and hole. Other reason also includes the probability for photo corrosion at the surface and transformation into bismuth carbonate during the photocatalytic studies. At high pH value, the above said reason may disappear and efficiency gets increases [23].

The variation of photocatalytic degradation efficiency of Gd-Bi_2O_3 for AV, RB, DY and RO dyes are depicted in *Figure 8*.

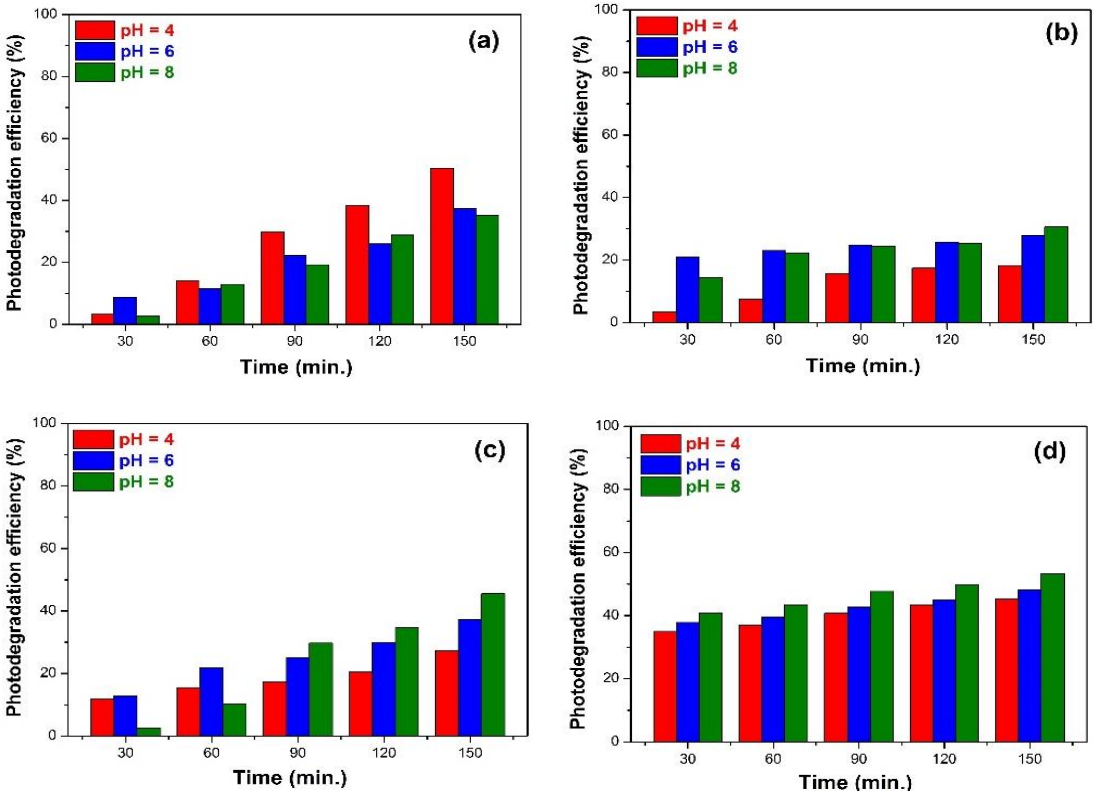

Fig. 7. Photocatalytic Efficiency of bare Bi_2O_3 for degradation of (a) AV, (b) RB, (c) DY and (d) RO.

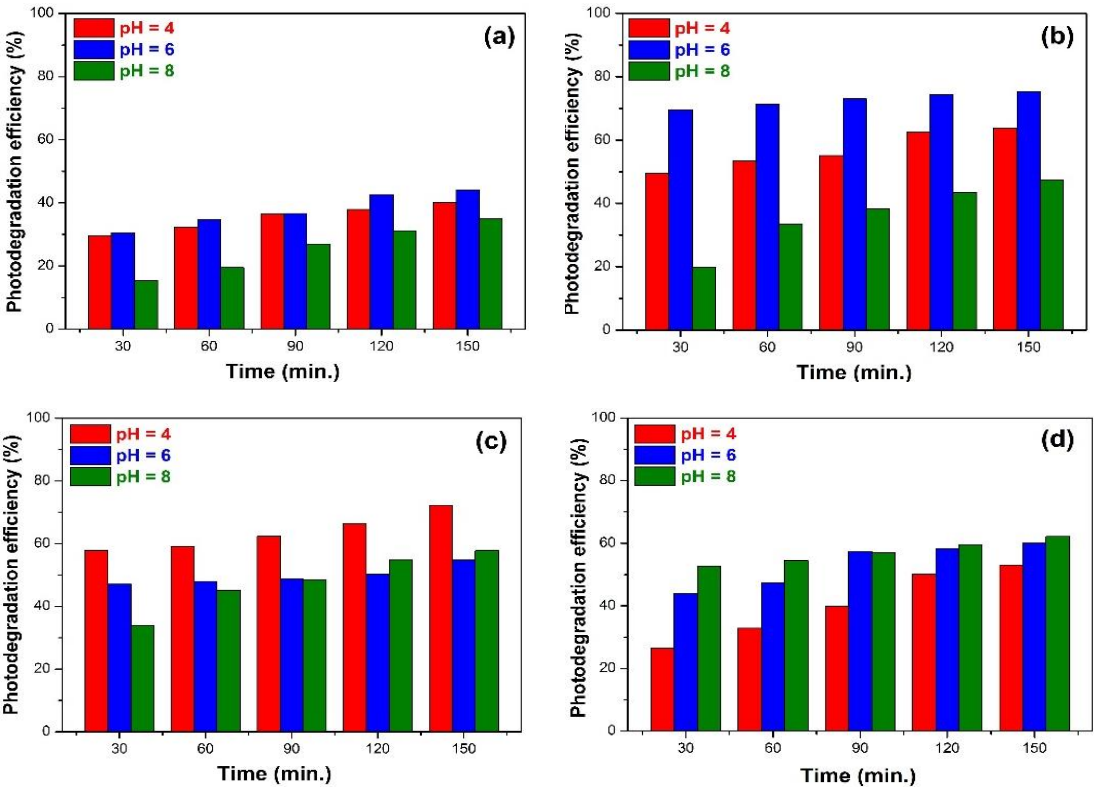

Fig. 8. Photocatalytic Efficiency of Gd-Bi_2O_3 for degradation of (a) AV, (b) RB, (c) DY and (d) RO.

Table 2 clearly depicts that, AV, RB, DY and RO were degraded to maximum percentage by the Gd-Bi_2O_3 photocatalyst for all pH values. The prompt explanation for the achievement of maximum degradation efficiency is, under acidic condition dye molecule can readily agglomerate on the surface of the catalyst. The rod like Gd- Bi_2O_3 structure having exterior surface with maximum surface area. The doped Gd^{3+} ions may present on surface or incorporated into the Bi^{3+} lattice, it can act as an electron sink for the reductive reaction and the formation of superoxide radical anion at the catalytic surface. Besides, Gd^{3+} ions present on the surface of the catalyst entertaining the electron-hole separation and delay the recombination of the same. As a result, the degradation efficiency of Gd-Bi_2O_3 is superior to bare Bi_2O_3 [24].

Table 1. Photocatalytic efficiency of bare Bi_2O_3 for selected dyes.

Dyes	Photocatalytic Efficiency of bare Bi_2O_3 %		
	pH - 4	pH - 6	pH - 8
Acid Violet-19	52	40	36
Rhodamine-B	20	28	34
Direct Yellow-8	28	38	48
Reactive Orange-16	46	50	56

3.5.1. Mechanism of Photocatalytic Degradation

The possible photodegradation mechanism was illustrated in *Figure 9*. Initially the catalyst was illuminated with UV light source. The catalyst absorbs the incident photons, leads to excitation of electron and transferred from valence band (VB) to conduction band (CB). As a result, photo induced electron and hole generated in VB and CB respectively. The photogenerated electron captured by the oxygen molecule resides in the vicinity of surface and gets reduced to super oxide radical anion ($^{\bullet}O_2^-$). Further, $^{\bullet}O_2^-$ may react with H^+ give $HO_2^{\bullet}$, which in turn accept an electron from catalytic surface results another oxidant H_2O_2. Subsequently, the hole on the surface of catalyst react with OH^- ions or H_2O molecule to form hydroxide radicals ($^{\bullet}OH$). All the produced super oxide radical anion ($^{\bullet}O_2^-$), hydroxide radicals ($^{\bullet}OH$) and H_2O_2 are strong oxidising species which can oxidise the dye molecules efficiently. Moreover, the efficiency of photodegradation merely depends on the catalytic surface area, narrow band gap, extent of separation of photo induced electron and hole [25].

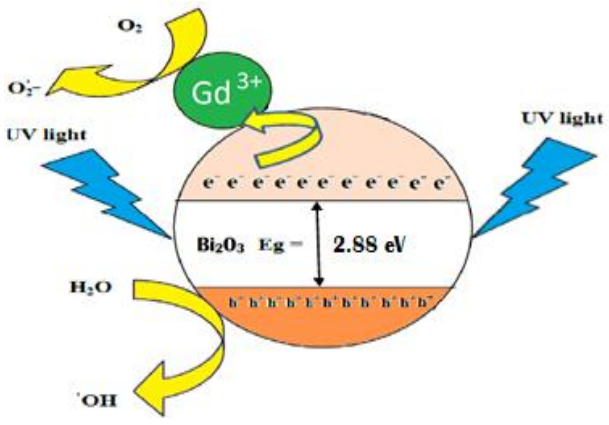

Fig. 9. Mechanism of Photocatalytic Degradation.

Table 2. Photocatalytic efficiency of Gd-Bi_2O_3 for selected dyes.

Dyes	Photocatalytic Efficiency of Gd-Bi_2O_3 %		
	pH - 4	pH - 6	pH - 8
Acid Violet-19	39	46	36
Rhodamine-B	64	76	48
Direct Yellow-8	72	56	60
Reactive Orange-16	54	60	64

$$Bi_2O_3 \rightarrow Bi_2O_3\,(e^-\,(CB) + h^+\,(VB)) \quad \text{‘(1)’}$$

$$O_2 + e- \rightarrow O_2^{\bullet-} \quad \text{‘(2)’}$$

$$O_2\bullet- + H^+ \rightarrow HO_2^{\bullet} \quad \text{‘(3)’}$$

$$HO_2^{\bullet} + e^- \rightarrow HO_2^- \quad \text{‘(4)’}$$

$$HO_2^- + H^+ \rightarrow H_2O_2 \quad \text{‘(5)’}$$

$$H_2O_2 + e^- \rightarrow OH^- + HO^{\bullet} \quad \text{‘(6)’}$$

$$HO^- + h^+ \rightarrow HO^{\bullet} \quad \text{‘(7)’}$$

$$\text{Dye Stuffs} + OH^{\bullet}/OH^- \rightarrow CO_2 + H_2O + \text{Simple products} \quad \text{‘(8)’}$$

In the case of Gd-Bi_2O_3, the presence of Gd ion replaces the Bi^{3+} in the lattice of Bi_2O_3 and can act as a photo sensitizer. The doped Gd ion at surface or in lattice of Bi_2O_3 can trap the photogenerated electron and get reduced. The reduced form of metal ions is highly unstable and transfer absorbed electron to the O_2 on the surface, leads to the formation of superoxide radical anion. On the other hand, it enhances the electron-hole separation as well as retard the recombination of the same. Thus, the rare earth metal ion (Gd^{3+} ion) doping approach explores and enhances the efficiency of the semiconductor photodegradation.

4. Conclusion

This paper reveals the synthesis of dominant exposed (120) phase of α-Bi_2O_3 nanoparticles by hydrothermal method. The existence of rectangular and nano-rod like structure, crystallinity and band gap was confirmed by standard characterization techniques. Furthermore, Gd-Bi_2O_3 photocatalysts exhibits obviously enhanced photocatalytic efficiency than the bare Bi_2O_3 towards the degradation of selected dyes under UV light irradiation. The enhanced photocatalytic activity of Gd-Bi_2O_3 was attributed by reducing the direct band gap of bare Bi_2O_3 by Gd^{3+} doping. This work can provide new insights in the synthesis of synergistic bismuth oxide with variant dopant and their applications for degradation of industrial effluents and other organic pollutants. However, it demands subsequent investigations and developments for practical applications.

References

[1] W. Raza, M. M. Haque, M. Muneer, T. Harada and M. Matsumura, J. Alloys. Compd. 648, 641 (2015); https://doi.org/10.1016/j.jallcom.2015.06.245

[2] "W. E. Mahmouda and A. A. Al-Ghamdia, Polym. Adv. Technol 22, 877 (2011); https://doi.org/10.1002/pat.1591

[3] A. M. N Jassim, S. A. Farhan, J.A.S.Salman, K.J. Khalaf, M.F. Al Marjani and M. T. Mohammed, Int. J. Chem. Biol. Sci. 1, 81 (2015)".

[4] M. J. Oviedo, O. E. Contreras, Y. Rosenstein, R .Vazquez Duhalt, Z. S. Macedo, G. G. Carbajal-Arizaga and G. A, J. Nanomater, 2016 (2016); https://doi.org/10.1155/2016/9782625

[5] M .Abudayyak, E . Oztas, M. Arici and G. Ozhan, Chemosphere, 169, 117 (2017); https://doi.org/10.1016/j.chemosphere.2016.11.018

[6] Y. Dai, L. Yin, J. Alloys Compd, 563, 80 (2013); https://doi.org/10.1016/j.jallcom.2013.02.105

[7] X. Gou, R .Li, G. Wang, Z. Chen and D. Wexler, Nanotechnology, 20, 495 (2009); https://doi.org/10.1088/0957-4484/20/49/495501

[8] S. Sood, A. Umar, S. Kumar Mehta, S. K Kansal, Ceramics International, 41(3), 3355- (2015); https://doi.org/10.1016/j.ceramint.2014.11.010

[9] M. Schlesinger, M. Weber, S. Schulze, M. Hietschold, M. Mehring, Chemistry, 2, 146 (2013); https://doi.org/10.1002/open.201300013

[10] J. Wu, Qin F, Lu Z, Yang HJ and Chen R, Nanoscale Res. Lett. 6, 66 (2011); https://doi.org/10.1186/1556-276X-6-66

[11] L. Torrisi, L. Silipigni, N. Restuccia, S. Cuzzocrea, M. Cutroneo, F. Barreca, B. Fazio, G. Di Marco and S. Guglielmino, J. Phys. Chem. Solids, 119, 62 (2018); https://doi.org/10.1016/j.jpcs.2018.03.034

[12] Z.A. Zulkifli, K.A. Razak, W.N. Rahman and S.Z. Abidin, J. Phys. Conf. Ser. 1082, 012103 (2018); https://doi.org/10.1088/1742-6596/1082/1/012103

[13] M. Mallahi, A. Shokuhfar, M.R Vaezi, A. Esmaeilirad and V. Mazinani, AJER 3, 162 (2014); https://doi.org/10.17950/ijer/v3s4/420

[14] G. Carotenuto, C.L. Hison, F. Capezzuto and M. Palomba, J. Nanoparticle, 11, 1729 (2009); https://doi.org/10.1007/s11051-008-9541-6

[15] J. Huang, Y.Q. Zheng, H.L. Zhu and J.J Wang. J. Solid State Chem. 239, 274 (2016); https://doi.org/10.1016/j.jssc.2016.05.006

[16] H. Kim, C. Jin, S. Park, W.I. Lee, I.J. Chin and C. Lee, Chem. Eng. J. 215, 15 (2013).

[17] T.P. Gujar, V.R. Shinde, C.D. Lokhande, R.S. Mane and S.H. Han, Appl. Surf. Sci. 252, 2747 (2006); https://doi.org/10.1016/j.apsusc.2005.04.034

[18] L. Mädler and S.E. Pratsinis, J. Am. Ceram Soc. 85, 1713 (2004); https://doi.org/10.1111/j.1151-2916.2002.tb00340.x

[19] A.P. Zhang, J.Z. Zhang, Chin. J. Inorg. Chem, 25, 2040 (2009)

[20] D.P. Dutta, M. Roy, A.K. Tyagi, Dalton Trans. 41, 10238 (2012); https://doi.org/10.1039/c2dt30653k

[21] Abdul Hameed, Valentina Gomba, Tiziano Montini, Laura Felisari, Paolo Fornasiero, Chemical Physics Letters,483, 254 (2009); https://doi.org/10.1016/j.cplett.2009.10.087

[23] L. Zhou, W. Wang, H. Xu, S. Sun, M. Shang, Chem. Eur. J. 15, 1776 (2009); https://doi.org/10.1002/chem.200801234

[24] Raza. Waseem., M.M. Haque, M. Muneer, T. Harada and M. Matsumura, Journal of Alloys and Compounds, 648, 641 (2015); https://doi.org/10.1016/j.jallcom.2015.06.245

[25] C.W. Tan, G.Q. Zhu, M. Hojamberdiev, K.S. Lokesh, X.C. Luo, L. Jin, J.P. Zhou, P. Liu,Y. Liu, J. Hazard. Mater. 278, 572 (2014); https://doi.org/10.1016/j.jhazmat.2014.06.019